Activation cross sections of proton-induced reactions on manganese up to 30 MeV

He Huang [a], Masayuki Aikawa [a,b,c], Damdinsuren Gantumur [a], Hiromitsu Haba [d]

[a] *Graduate School of Biomedical Science and Engineering, Hokkaido University, Sapporo 060-8638, Japan*

[b] *Faculty of Science, Hokkaido University, Sapporo 060-0810, Japan*

[c] *Global Center for Biomedical Science and Engineering, Faculty of Medicine, Hokkaido University, Sapporo 060-8648, Japan*

[d] *Nishina Center for Accelerator-Based Science, RIKEN, Wako 351-0198, Japan*

Abstract

The excitation functions of the ^{55}Mn(p,x)^{51}Cr, ^{54}Mn reactions were measured up to 30-MeV proton energy. The experiment was performed at the RIKEN AVF cyclotron using the stacked-foil activation technique. High-purity germanium (HPGe) detectors were used for the gamma-ray spectrometry. Obtained results were compared with previous experimental data and the prediction of the TALYS nuclear reaction model code available in the TENDL-2021 library. Physical thick target yields of ^{51}Cr and ^{54}Mn were derived from the measured cross sections.

Keyword

Manganese target, Activation products, proton-induced reaction, Excitation function

1. Introduction

Manganese has been widely used as an important chemical composition of ferritic steels used for reactor pressure vessels, and as mechanical properties of stainless steels used in nuclear facilities [1]. The manganese metal is also an important component to strengthen aluminum alloys, which are used in accelerator technology [2]. The alloys containing manganese work under irradiation and the reactions of manganese are worthy to be investigated.

Manganese is a monoisotopic element, and composed of one stable isotope ^{55}Mn. This facilitates the study of cross sections on the monoisotopic target ^{55}Mn without isotope enrichment. The cross sections are of great significance for thin layer activation technology, radionuclide production, the development of nuclear reaction model codes and so on [3].

Proton-induced reactions on manganese can produce some radionuclides used for application. The radionuclide ^{51}Cr produced from the reactions, with a half-life of $T_{1/2}$ = 27.8 d, decays by an electron capture accompanied by the emission of gamma rays of 320 keV. Chromium is essential element in blood cells, thus the radioactive ^{51}Cr was used for the labeling of red blood cells, which contributed to the measurement of the mass and volume of living systems [4, 5]. The ^{51}Cr-labeled albumin can also be used for the detection of protein loss in the gastrointestinal tract [6, 7]. Another radionuclide produced in the reactions, ^{52g}Mn, with a half-life of $T_{1/2}$ = 5.6 d, decays by electron capture and positron emission. It is also a medical radioisotope, which can be used in positron emission tomography (PET) [8, 9]. The radionuclide ^{54}Mn with a rather long half-life of 312.3 d, decays by electron capture and emits a single gamma ray of 834.8 keV. This appropriate property makes ^{54}Mn to be a standard test source for the calibration of the gamma-ray detectors [10].

In this work, we focused on proton-induced reactions on manganese. In the literature survey using the EXFOR library [11], we found several studies published earlier [12-19] below 30 MeV, where the peaks of the production cross sections of ^{51}Cr and ^{54}Mn are located. The experimental data of Levkovskii (1991) [11] were required to be normalized by a factor, for which 0.82 was adopted [20]. The comparison of the experimental data showed that the peak amplitudes of the experimental data were inconsistent.

Therefore, in this research, we measured the activation cross sections of the proton-induced reaction on ^{55}Mn. The results were compared with the former published experimental values, and also theoretical calculation values based on the TALYS code derived from the TENDL-2021 data library [21]. This study is expected to contribute to the production of radionuclides for applications and the development of theoretical model codes.

2. Material and methods

For the measurements of excitation functions of the proton-induced reactions on manganese targets up to 30 MeV, we adopted the well-known and established stacked-foil activation technique. The experiment was performed at the AVF cyclotron of the RIKEN RI Beam Factory, Wako, Japan.

The stacked target consisted of thin foils of manganese alloy, pure titanium and aluminum. The manganese alloy consisted of copper, manganese, and nickel, which was expected to preserve uniformity in both thickness and elemental ratio. To take into account the influence of manganese alloy composition on the experimental results, we analyzed the elemental ratio of the manganese alloy foil before irradiation. A scanning electron microscopy with energy dispersive spectroscopy using a microscope (Hitachi TM4000 Plus II) was performed, and the mass ratio of the components in the manganese alloy was found to be Mn 12.5%, Cu 85.2% and Ni 2.2%. The natural titanium foil (99.6% purity, Nilaco Corp., Japan) was used for the ^{nat}Ti(p,x)^{48}V monitor reaction to assess beam parameters and target thicknesses. The monoisotopic element ^{27}Al foil (>99% purity, Nilaco Corp., Japan) was interleaved for energy degradation and collection of the recoiled products produced from the Ti foils adjacent at the upstream of the beam. The configuration of the stacked target was seventeen sets of Mn-Mn-Ti-Ti-Al foils. Only gamma spectra from second foils of manganese alloy and Ti were measured assuming compensation of recoiled products. The average thicknesses of the foils were derived before cutting to small foils, which were 24.6, 8.70, and 13.8 mg/cm^2 for manganese alloy, Ti, and Al foils, respectively. The foils were cut into a size of 8 × 8 mm to fit a target holder. The target holder also served as a Faraday cup.

The target was irradiated for 20 minutes with a proton beam collimated to a 3 mm diameter.

The average beam intensity measured by the Faraday cup was 182 nA. The primary beam energy determined by the time-of-flight method [22] was 30.1±0.1 MeV. The attenuation of energy in each foil was calculated by stopping powers obtained from the SRIM code [23].

The high-resolution gamma-ray spectrometry was performed using two HPGe detectors (two ORTEC GEM30P4-70) and the analysis software (SEIKO EG&G Gamma Studio). The efficiency of the detectors was calibrated using a gamma-ray point source consisting of ^{57,60}Co, ^{85}Sr, ^{88}Y, ^{109}Cd, ^{113}Sn, ^{137}Cs, ^{139}Ce, ^{203}Hg, and ^{241}Am (Eckert & Ziegler Isotope Products). The related gamma lines were shown in Table 1, which were retrieved from the online databases, NuDat 3.0 [24], LiveChart [25], Lund/LBNL Nuclear Data Search [26] and QCalc [27].

Table 1. Reaction and decay data retrieved from online databases

Nuclide	Half-life	Decay mode (%)	E_γ (keV)	I_γ (%)	Contributing reaction	Q-value (MeV)	Threshold (MeV)
^{51}Cr	27.7 d	EC: 100	**320.08244**	9.911	^{55}Mn(p,nα)	-9.5	9.6
					^{55}Mn(p,dt)	-27.1	27.6
					^{55}Mn(p,npt)	-29.3	29.8
^{54}Mn	312.20 d	EC+β^+: 100	**834.848**	99.976	^{55}Mn(p,d)	-8.0	8.1
		β^-: 0.93×10^{-4}			^{55}Mn(p,np)	-10.2	10.4
^{48}V	15.97d	EC+β^+: 100	**983.53**	99.98	^{47}Ti(p,γ)	6.8	0
			511.0	99.8	^{48}Ti(p,n)	-4.8	4.9
			1312.106	98.2	^{49}Ti(p,2n)	-12.9	13.2
					^{50}Ti(p,3n)	-23.9	24.4

We used the following well-known equation [28] to derive the cross sections:

$$\sigma = \frac{N\lambda}{n_T I \varepsilon_d \varepsilon_\gamma \varepsilon_t (1 - e^{-\lambda T_b}) e^{-\lambda T_c} (1 - e^{-\lambda T_m})}$$

where σ is the cross section (cm^2), N is the net count of the characteristic gamma-line, λ is the decay constant of the radioisotope (s^{-1}), n_T is the atomic number areal density of the target (cm^{-2}), I is the deuteron-beam intensity (s^{-1}), ε_d, ε_γ, and ε_t are the efficiency of the HPGe detector, gamma-line branching ratio, and dead time correction, respectively. T_b, T_c, and T_m are the irradiation, cooling, and measurement times (s), respectively.

To assess the beam parameters and target thicknesses, the cross sections of the ^{nat}Ti(p,x)^{48}V monitor reaction were derived. We used net counts of the gamma line at 983.5 keV (I_γ = 99.98%) emitted from second Ti foils to derive the cross sections. The derived cross sections were compared with the recommended data of IAEA [29, 30]. According to the comparison with the recommended values in 2007 [29], the peak position of our excitation function curve was shifted to higher energy. To fit the peak position, the foil thicknesses and the primary beam energy was corrected within uncertainties by +1% and -0.1 MeV, respectively. The corrected thicknesses and beam energy were 24.8, 8.79, and 13.9 mg/cm^2 for manganese alloy, Ti, and Al foils and 30 MeV, respectively. The measured beam intensity was adopted without any correction. The cross sections of the monitor reaction using the corrected parameters are compared with the recommended values in Fig. 1.

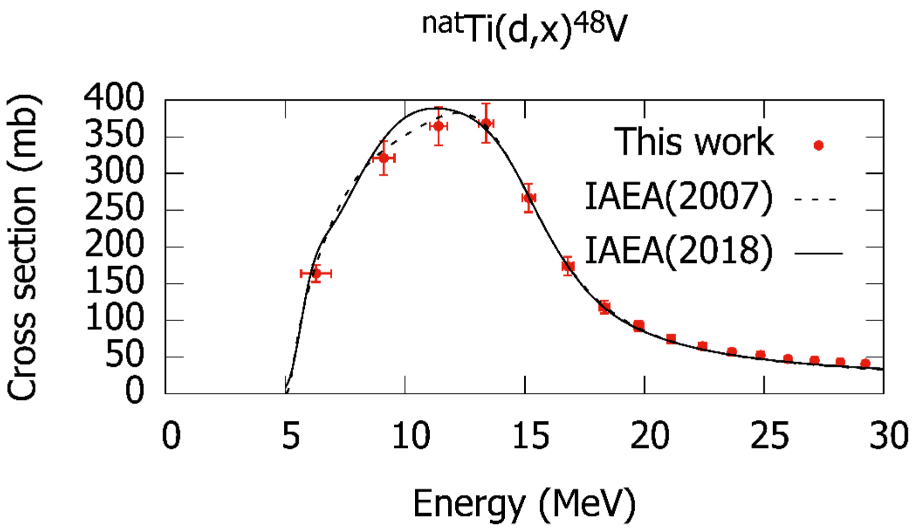

Fig. 1. The cross sections of the monitor reaction compared with the recommended values of IAEA [29, 30]

We performed four series of measurements of the second manganese alloy foils to determine the cross sections of different radionuclides with different half-lives. The information related to our measurement were shown in Table 2. The fourth measurement was performed long after irradiation for the long-lived radionuclide ^{54}Mn. We compared the consistency of the cross sections among the four series, and the cross sections derived from one measurement series with the proper cooling time were given in the result part.

Table 2. Measurement information

Series	Distance	Cooling time	Dead time
Ser. 1	15 cm	18.4-21.1 h	0.1-2.6%
Ser. 2	5-30 cm	22.8-31.3 h	<3.6%
Ser. 3	5 cm	52.8-76.9 h	0.5-3.2%
Ser. 4	5 cm	120-121 d	<0.1%

The total relative uncertainties were calculated by the square root of the summed squares of each uncertainty, as the following equation [31]

$$\frac{\Delta\sigma}{\sigma} = \sqrt[2]{\left(\frac{\Delta n_T}{n_T}\right)^2 + \left(\frac{\Delta I}{I}\right)^2 + \left(\frac{\Delta p}{p}\right)^2 + \left(\frac{\Delta \varepsilon_d}{\varepsilon_d}\right)^2 + \left(\frac{\Delta \varepsilon_\gamma}{\varepsilon_\gamma}\right)^2 + \left(\frac{\Delta N}{N}\right)^2}$$

where Δn_T, ΔI, Δp, $\Delta\varepsilon_d$, $\Delta\varepsilon_\gamma$, and ΔN are the uncertainties coming from target thickness (1%), beam intensity (5%), mass ratio (3.3%), detector efficiency (5%), gamma-ray branching ratio (<0.9%), and counting statistics (0.5–44.8%), respectively. The estimated total uncertainties of cross sections are 7.9-45.5%.

3. Results and discussion

The production cross sections with total uncertainties are listed in Table 3 and displayed in Fig. 2 and 3 with the previously published data [12-19] and theoretical prediction data retrieved from the TENDL-2021 library [21]. The experimental data of Levkovskii (1991) [11] were normalized by the factor of 0.82, because of the deviation of the $^{nat}Mo(p,x)^{96}Tc$ monitor reaction [20]. Contributions from copper and nickel in the target material were considered using the theoretical values of TENDL-2021 [21].

Table 1. Production cross sections (mb) in the $^{55}Mn(p,x)$ reactions.

Energy (MeV)	^{51}Cr	^{54}Mn
29.6±0.1	76.5±6.5	370±27
28.5±0.1	75.9±6.4	391±28
27.5±0.1	81.2±6.8	436±32
26.4±0.1	81.5±6.5	458±33
25.2±0.1	75.0±6.0	491±36
24.0±0.1	68.4±5.1	499±36
22.8±0.2	58.7±5.1	494±36
21.5±0.2	51.3±5.3	487±35
20.2±0.2	41.0±4.3	451±33
18.8±0.2	21.4±3.1	392±28
17.3±0.2	7.96±2.57	320±23
15.7±0.3		218±16
14.0±0.3		92.6±6.9
12.0±0.3		7.91±0.79

3.1. Formation of the ^{51}Cr radionuclide

The spectra were measured after the cooling time of 52.8 hours. The cross sections of ^{51}Cr production were derived using the gamma line at 320.0824 keV (I_γ = 9.91%). The ^{51}Cr is mainly produced by the $^{55}Mn(p,n\alpha)^{51}Cr$ reaction in our energy range due to its rather low threshold energy of 9.6 MeV. The other channels of the $^{55}Mn(p,dt)^{51}Cr$ and $^{55}Mn(p,npt)^{51}Cr$ reactions have threshold energies of 27.6 and 29.8 MeV, respectively. The copper in the target material never produces ^{51}Cr nor its parent nuclide ^{51}Mn according to the threshold energy. The other alloy component nickel has a reaction channel $^{58}Ni(p,2\alpha)^{51}Mn$ with a low threshold energy of 9.7 MeV, but its cross sections reach 0.22 mb at 30 MeV according to TENDL-2021 and were negligible.

The derived cross sections are shown in Fig. 2 in comparison with the former experiment data [12-17] and the theoretical prediction of TENDL-2021 [21]. The cross sections recommended by IAEA [32] using six selected experimental datasets [12-16, 33] are also included in Fig. 2, which are higher than our result above 22 MeV. The data of Michel et al. (1997) [14] and the normalized data of Levkovskii (1991) [11] above 22 MeV are consistent with our data. The other experimental data at around the peak are larger than ours. The TENDL-2021 underestimates the cross sections above 17 MeV.

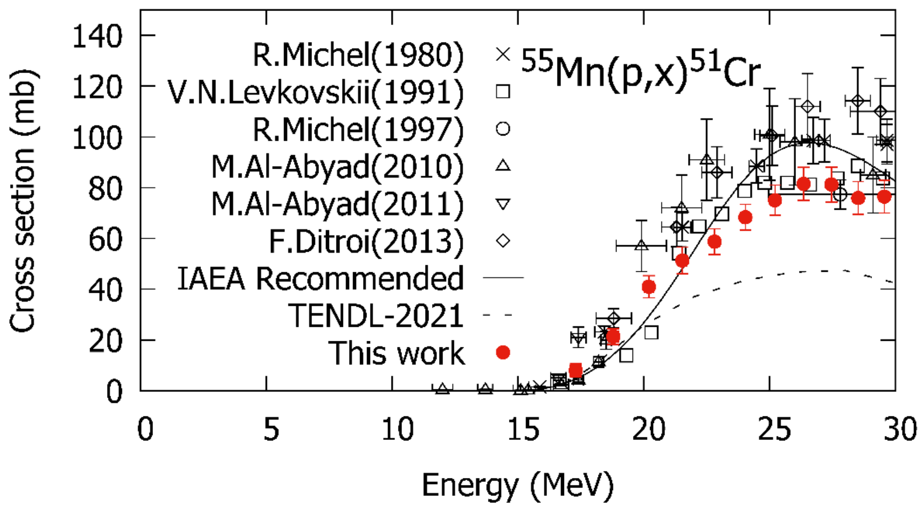

Fig. 2 Cross sections of the $^{55}Mn(p,x)^{51}Cr$ reaction with the previous data [12-17, 32] and the TENDL-2021 [21].

3.2. Formation of the ^{54}Mn radionuclide

We adopted a longer cooling time of 120 days to determine the cross sections of ^{54}Mn. The photopeak area of the gamma line at 834.848 keV (I_γ = 99.976%) was counted. The ^{54}Mn was produced by the $^{55}Mn(p,d)$ and $^{55}Mn(p,np)$ reactions with threshold energy of 8.1 and 10.4 MeV, respectively. The alloy component ^{63}Cu could generate ^{54}Mn through $^{63}Cu(p,d2\alpha)$ (E_{th} = 21.0 MeV) and $^{63}Cu(p,np2\alpha)$ reactions (E_{th} = 23.3 MeV), but the cross sections of the reactions are negligibly small below 30 MeV according to TENDL-2021 [21]. The contribution of the other alloy component nickel was also negligible according to the abundance and predicted cross sections in TENDL-2021.

Our result is shown in Fig. 3 and compared with the formerly published data [12-19] and the theoretical prediction of TENDL-2021 [21]. The experimental data of Levkovskii (1991) [11] normalized by the factor 0.82 [20] and the prediction values of TENDL-2021 [21] are consistent with our result, while the most data of the other studies are higher than our data.

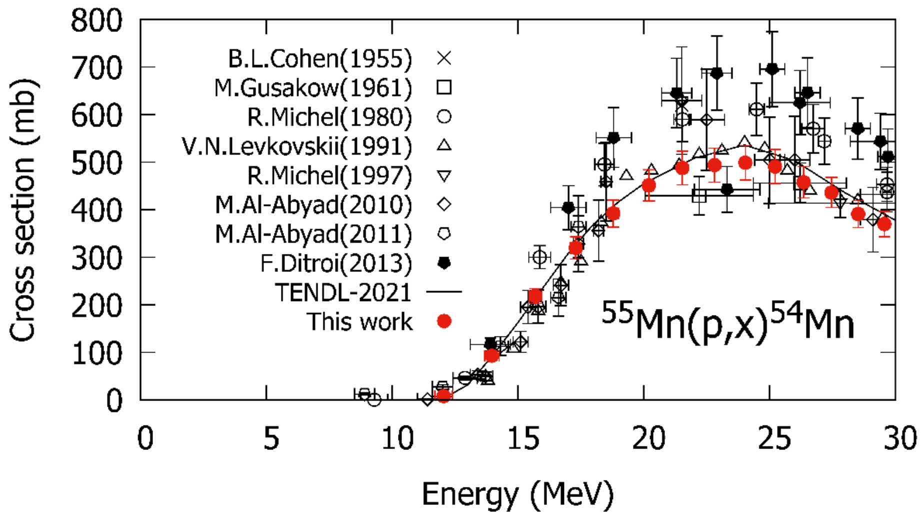

Fig. 3 Cross sections of the $^{55}Mn(p,x)^{54}Mn$ reaction with the previous data [12-19] and the TENDL-2021 [21].

3.3. Formation of the ^{52g}Mn radionuclide and effect of iron contamination

The ground state ^{52g}Mn has a half-life of 5.591 days and is produced by the $^{55}Mn(p,nt)^{52g}Mn$ reaction above its threshold energy at 23.2 MeV. The photopeak area of the gamma line at 935.538 keV (I_γ = 94.5%) was counted. We used the spectra measured after the cooling time of 52.8 hours to derive its production cross sections. The metastable state ^{52m}Mn ($J^\pi = 2^+$) with a short half-life of 21.1 min decays to the ground state by the isomeric transition with a small branching ratio of 1.78%. The metastable state ^{52m}Mn decayed before measurements and the net counts contained the contribution of ^{52m}Mn decay. Copper, a component of the manganese alloy, cannot produce $^{52g,52m}Mn$ in the energy region. ^{58}Ni, the most abundant isotope of another component nickel, contributes negligibly small cross sections to produce $^{52g,52m}Mn$ according to TENDL-2021 [21].

The derived cross sections of the $^{55}Mn(p,x)^{52g}Mn$ reaction were compared with the formerly published data [12, 14, 16] and the theoretical prediction of TENDL-2021. Our results were much higher than the experimental and theoretical values. In addition, some data points existed below the threshold energy of the $^{55}Mn(p,nt)^{52g}Mn$ reaction. This would be due to iron contamination that was unmeasurable in our elemental analysis. According to the comparison of the derived cross sections with experimental ones of proton bombardment on iron [34], we found that the shape of the excitation function was consistent and the possible iron contamination was 0.7% at maximum. Therefore, the cross sections of the $^{55}Mn(p,nt)^{52g}Mn$ reaction could not be derived. The contaminant less affects the other cross sections for ^{54}Mn and ^{51}Cr production because of the low mass ratio (Fe/Mn < 0.056) and smaller cross sections below 30 MeV.

3.4. Thick target yields of ^{51}Cr and ^{54}Mn

We calculated thick target yields of ^{51}Cr and ^{54}Mn from the derived cross sections. The results are shown in Fig. 4 and Fig. 5 as a function of proton energy. The thick target yields of ^{51}Cr reaches 981.3 MBq/C at 29.6 MeV. Our result curve in good agreement with the former experimental results of Dmitriev et al. (1983) [35]. The yield calculated from the recommended cross sections of $^{55}Mn(p,x)^{51}Cr$ could also be exported from the IAEA [32], and compared with our results. The recommended yields are higher than ours at energy higher than 24.2 MeV, and reach 1147 MBq/C at 30 MeV.

The longer-lived ^{54}Mn could be generated and its yields reach about 713.1 MBq/C at 29.6 MeV, although chemical separation is difficult for its application production. The thick target yields of ^{54}Mn derived from our data were little higher than the two former results of Krasnov(1966) [36] and Dmitriev(1983) [35].

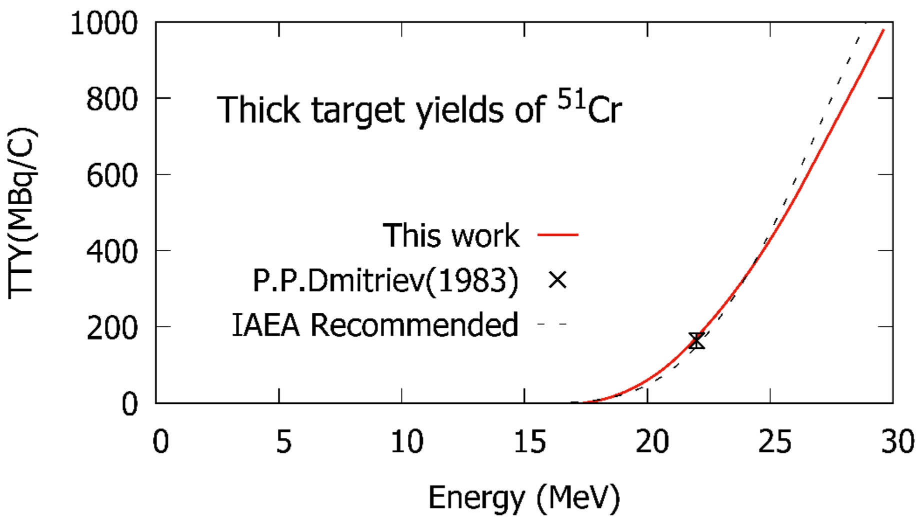

Fig. 4. Thick target yields of ^{51}Cr.

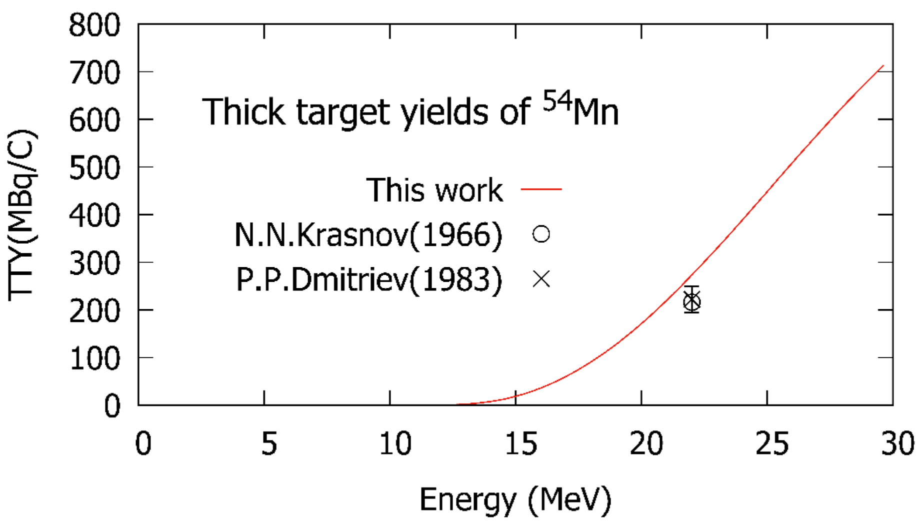

Fig. 5. Thick target yields of ^{54}Mn.

4. Summary

The excitation function measurement for the proton-induced reactions on ^{55}Mn was performed up to 30 MeV at the RIKEN AVF cyclotron. The stacked-foil activation technique and high-resolution gamma-ray spectrometry were used for this experiment. The production cross sections of ^{51}Cr and ^{54}Mn were measured. The derived data were compared with the theoretical values of TENDL-2021 and the previously published data. The obtained results can contribute to applications and the development of nuclear reaction model codes.

Acknowledgment

This work was carried out at RI Beam Factory operated by RIKEN Nishina Center and CNS, University of Tokyo, Japan.

Reference

1. D. Féron, 2 - Overview of nuclear materials and nuclear corrosion science and engineering. Woodhead Publ. series in energy, (2012) 31-56 https://doi.org/10.1533/9780857095343.1.31.
2. R.A. Michelotti, R.A. Tennant, N.K. Bultman, J.L. Uher, R.J. Brewton, A. Mayer, Materials Considerations for a High Power-Density Accelerator. IEEE Trans. Nucl. Sci. 32(1985) 2849-2851 https://doi.org/10.1109/TNS.1985.4334202.
3. M.U. Khandaker, K. Kim, M.W. Lee, K.S. Kim, G.N. Kim, Y.S. Cho, Y.O. Lee, Production cross-sections for the residual radionuclides from the natCd(p, x) nuclear processes. Nuclear Instruments and Methods in Physics Research Section B: Beam Interactions with Materials and Atoms. 266(2008) 4877-4887 https://doi.org/10.1016/j.nimb.2008.08.014.
4. S.J. Gray, K. Sterling, The tagging of red cells and plasma proteins with radioactive chromium. J. Clin. Invest. 29(1950) 1604-13 https://doi.org/10.1172/JCI102403.
5. A.B. Willett, V.V. Grantham, Determination of hemolytic anemia through the study of ^{51}Cr red cell survival and splenic sequestration. J. Nucl. Med. Technol. 36(2008) 95-8 https://doi.org/10.2967/jnmt.107.049023.
6. T.A. Waldmann, R.D. Wochner, W. Strober, The role of the gastrointestinal tract in plasma protein metabolism. Am. J. Med. 46(1969) 275-285 https://doi.org/10.1016/0002-9343(69)90011-4.
7. R.M. Kerr, J.J. Du Bois, P.R. Holt, Use of ^{125}I- and ^{51}Cr-labeled albumin for the measurement of gastrointestinal and total albumin catabolism. J. Clin. Invest. 46(1967) 2064-2082 https://doi.org/10.1172/JCI105694.
8. M. Pagani, S. Stone-Elander, S.A. Larsson, Alternative positron emission tomography with non-

conventional positron emitters: effects of their physical properties on image quality and potential clinical applications. Eur. J. Nucl. Med. 24(1997) 1301-27 https://doi.org/10.1007/s002590050156.

9. C.M. Lewis, S.A. Graves, R. Hernandez, H.F. Valdovinos, T.E. Barnhart, W. Cai, M.E. Meyerand, R.J. Nickles, M. Suzuki, ^{52}Mn production for PET/MRI tracking of human stem cells expressing divalent metal transporter 1 (DMT1). Theranostics. 5(2015) 227-39 https://doi.org/10.7150%2Fthno.10185v.

10. L.M. Cavallo, B.M. Coursey, S.B. Garfinkel, J.M.R. Hutchinson, W.B. Mann, Needs for radioactivity standards and measurements in different fields. Nucl. Instrum. Methods. 112(1973) 5-18 https://doi.org/10.1016/0029-554X(73)90768-4.

11. N. Otuka, E. Dupont, V. Semkova, B. Pritychenko, A.I. Blokhin, M. Aikawa, S. Babykina, M. Bossant, G. Chen, S. Dunaeva, R.A. Forrest, T. Fukahori, N. Furutachi, S. Ganesan, Z. Ge, O.O. Gritzay, M. Herman, S. Hlavač, K. Katō, B. Lalremruata, Y.O. Lee, A. Makinaga, K. Matsumoto, M. Mikhaylyukova, G. Pikulina, V.G. Pronyaev, A. Saxena, O. Schwerer, S.P. Simakov, N. Soppera, R. Suzuki, S. Takács, X. Tao, S. Taova, F. Tárkányi, V.V. Varlamov, J. Wang, S.C. Yang, V. Zerkin, Y. Zhuang, Towards a More Complete and Accurate Experimental Nuclear Reaction Data Library (EXFOR): International Collaboration Between Nuclear Reaction Data Centres (NRDC). Nucl. Data Sheets. 120(2014) 272-276 https://doi.org/10.1016/j.nds.2014.07.065.

12. R. Michel, G. Brinkmann, On the depth-dependent production of radionuclides ($44 \leq A \leq 59$) by solar protons in extraterrestrial matter. J. Radioanal. Nucl. Chem. 59(1980) 467-510 https://doi.org/10.1007/BF02517298.

13. V.N. Levkovskii, Cross sections of medium mass nuclide activation (A= 40-100) by medium energy protons and alpha-particles (E= 10-50 MeV). Inter-Vesi, Moscow, USSR. 1991

14. R. Michel, R. Bodemann, H. Busemann, R. Daunke, M. Gloris, H.J. Lange, B. Klug, A. Krins, I. Leya, M. Lüpke, S. Neumann, H. Reinhardt, M. Schnatz-Büttgen, U. Herpers, T. Schiekel, F. Sudbrock, B. Holmqvist, H. Condé, P. Malmborg, M. Suter, B. Dittrich-Hannen, P.W. Kubik, H.A. Synal, D. Filges, Cross sections for the production of residual nuclides by low- and medium-energy protons from the target elements C, N, O, Mg, Al, Si, Ca, Ti, V, Mn, Fe, Co, Ni, Cu, Sr, Y, Zr, Nb, Ba and Au. Nucl. Instrum. Methods Phys. Res. B: Beam Interact. Mater. At. 129(1997) 153-193 https://doi.org/10.1016/S0168-583X(97)00213-9.

15. M. Al-Abyad, I. Spahn, S.M. Qaim, Experimental studies and nuclear model calculations on proton induced reactions on manganese up to 45 MeV with reference to production of ^{55}Fe, ^{54}Mn and ^{51}Cr. Appl Radiat Isot. 68(2010) 2393-7 https://doi.org/10.1016/j.apradiso.2010.06.013.

16. F. Ditrói, F. Tárkányi, S. Takács, A. Hermanne, H. Yamazaki, M. Baba, A. Mohammadi, Activation cross-sections of longer lived products of proton induced nuclear reactions on manganese up to 70MeV. Nucl. Instrum. Methods Phys. Res. B: Beam Interact. Mater. At. 308(2013) 34-39 https://doi.org/10.1016/j.nimb.2013.04.058.

17. M. Al-Abyad, H. EL-Showaimy, M. Challan, A. Khalaf, M. Comsan, Experimental Investigation and Nuclear Model Calculations of Radionuclides Produced by Proton Induced Reactions on In and

Mn Targets at Low Energy. AJNSA. 44(2011) 111-121

18. B.L. Cohen, E. Newman, (p, pn) and (p, 2n) Cross Sections in Medium Weight Elements. Phys. Rev. 99(1955) 718-723 https://doi.org/10.1103/PhysRev.99.718.
19. M. Gusakow, G. Albouy, N. Poffé, C. Riehl, Réactions (p, pn) à moyenne énergie. J. phys. Radium. 22(1961) 636-638 https://doi.org/10.1051/jphysrad:019610022010063600.
20. S.M. Qaim, S. Sudar, B. Scholten, A.J. Koning, H.H. Coenen, Evaluation of excitation functions of ^{100}Mo(p,d+pn)^{99}Mo and ^{100}Mo (p,2n)^{99m}Tc reactions: Estimation of long-lived Tc-impurity and its implication on the specific activity of cyclotron-produced ^{99m}Tc. Appl Radiat Isot. 85(2014) 101-13 https://doi.org/10.1016/j.apradiso.2013.10.004.
21. A.J. Koning, D. Rochman, Modern Nuclear Data Evaluation with the TALYS Code System. Nucl. Data Sheets. 113(2012) 2841-2934 https://doi.org/10.1016/J.NDS.2012.11.002.
22. T. Watanabe, M. Fujimaki, N. Fukunishi, H. Imao, O. Kamigaito, M. Kase, M. Komiyama, N. Sakamoto, K. Suda, M. Wakasugi, K. Yamada, Beam energy and longitudinal beam profile measurement system at the RIBF. in: ,Proc. 5th Int. Part. Accel. Conf. (IPAC 2014), (2014) 3566–3568
23. J.F. Ziegler, J.P. Biersack, M.D. Ziegler. SRIM: the Stopping and Range of Ions in Matter. 2008; Available from: http://www.srim.org.
24. National Nuclear Data Center, information extracted from the NuDat database, NuDat 3.0. Available from: https://www.nndc.bnl.gov/nudat/.
25. International Atomic Energy Agency, LiveChart of Nuclides. 2009; Available from: https://wwwnds.iaea.org/livechart/.
26. S.Y.F. Chu, L.P. Ekström, R.B. Firestone. The Lund/LBNL Nuclear Data Search. 1999; Available from: http://nucleardata.nuclear.lu.se/toi/.
27. B. Pritychenko, A. Sonzogni. Q-value Calculator (QCalc). 2003; Available from: http://www.nndc.bnl.gov/qcalc/.
28. M.U. Khandaker, K. Kim, M.-W. Lee, K.-S. Kim, G. Kim, N. Otuka, Investigations of 89Y(p,x)86,88,89gZr, 86m+g,87g,87m,88gY, 85gSr, and 84gRb nuclear processes up to 42MeV. Nucl. Instrum. Methods Phys. Res. B: Beam Interact. Mater. At. 271(2012) 72-81 https://doi.org/10.1016/j.nimb.2011.11.009.
29. F. Tárkányi, S. Takács, K. Gul, A. Hermanne, M.G. Mustafa, M. Nortier, P. Obložinský, B. S.M. Qaim, Scholten, Y.N. Shubin, Z. Yousiang. Monitor Reactions 2007, updated version of charged particle crosssection database for medical radioisotope production, IAEA-TECDOC-1211. 2007; Available from: https://wwwnds.iaea.org/medical/medical-old/monitor_reactions.html.
30. A. Hermanne, A.V. Ignatyuk, R. Capote, B.V. Carlson, J.W. Engle, M.A. Kellett, T. Kibédi, G. Kim, F.G. Kondev, M. Hussain, O. Lebeda, A. Luca, Y. Nagai, H. Naik, A.L. Nichols, F.M. Nortier, S. V.Suryanarayana, S. Takács, F.T. Tárkányi, M. Verpelli, Reference Cross Sections for Charged-particle Monitor Reactions. Nucl. Data Sheets. 148(2018) 338-382 https://doi.org/10.1016/j.nds.2018.02.009.

31. N. Otuka, B. Lalremruata, M.U. Khandaker, A.R. Usman, L.R.M. Punte, Uncertainty propagation in activation cross section measurements. Radiat. Phys. Chem. 140(2017) 502-510 https://doi.org/10.1016/j.radphyschem.2017.01.013.
32. F.T. Tárkányi, A.V. Ignatyuk, A. Hermanne, R. Capote, B.V. Carlson, J.W. Engle, M.A. Kellett, T. Kibedi, G.N. Kim, F.G. Kondev, M. Hussain, O. Lebeda, A. Luca, Y. Nagai, H. Naik, A.L. Nichols, F.M. Nortier, S.V. Suryanarayana, S. Takács, M. Verpelli, Recommended nuclear data for medical radioisotope production: diagnostic gamma emitters. J. Radioanal. Nucl. Chem. 319(2019) 487-531 https://doi.org/10.1007/s10967-018-6142-4.
33. R. Stueck, Proton induced reactions on Ti, V, Mn, Fe, Co and Ni Measurement and hybrid model analysis of integral excitation functions and their application in model calculation for the production of cosmogenic nuclides. (1983)
34. K. Kim, M.U. Khandaker, H. Naik, G. Kim, Excitation functions of proton induced reactions on natFe in the energy region up to 45MeV. Nucl. Instrum. Methods Phys. Res. B: Beam Interact. Mater. At. 322(2014) 63-69 http://dx.doi.org/10.1016/j.nimb.2013.12.031.
35. P.P.Dmitriev, G.A.Molin, Radionuclide yields for thick targets at 22 MeV proton energy. Rept: USSR report to the I.N.D.C. 188(1983)
36. N.N.Krasnov, P.P.Dmitriev, Yields of nuclear reactions used for preparing ^{54}Mn in a cyclotron. Sov. At. Energy. 21(1966) 678

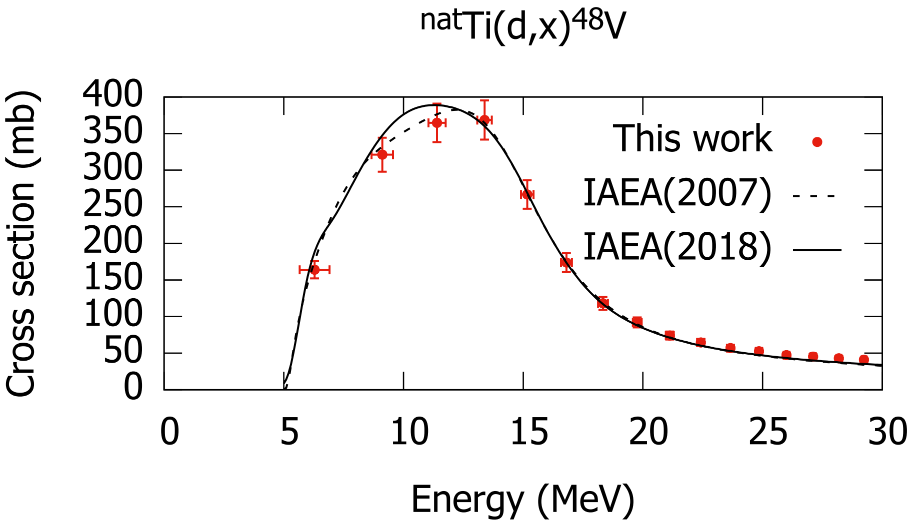

natTi(d,x)48V
Cross section (mb)
400
350
300
250
200
150
100
50
0
0
5
10
15
20
25
30
Energy (MeV)
This work
IAEA(2007)
IAEA(2018)

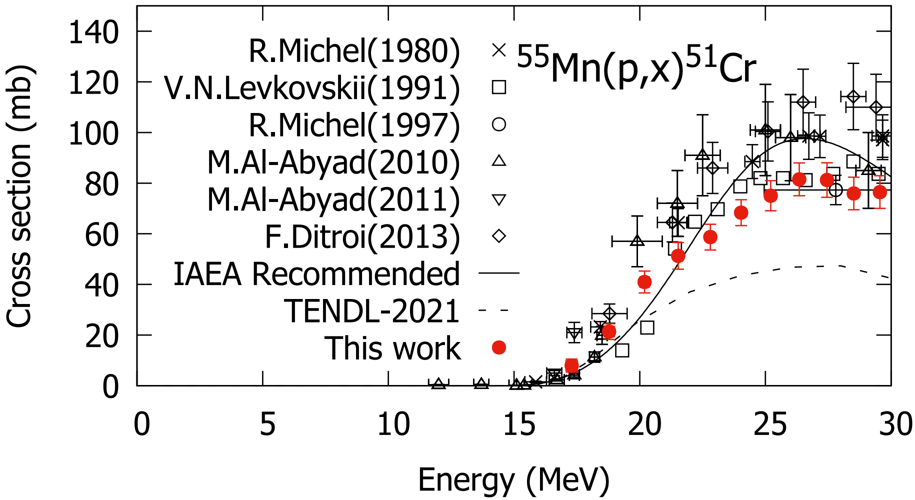

^{55}Mn(p,x)^{51}Cr
R.Michel(1980)
V.N.Levkovskii(1991)
R.Michel(1997)
M.Al-Abyad(2010)
M.Al-Abyad(2011)
F.Ditroi(2013)
IAEA Recommended
TENDL-2021
This work
Cross section (mb)
Energy (MeV)
0
20
40
60
80
100
120
140
0
5
10
15
20
25
30

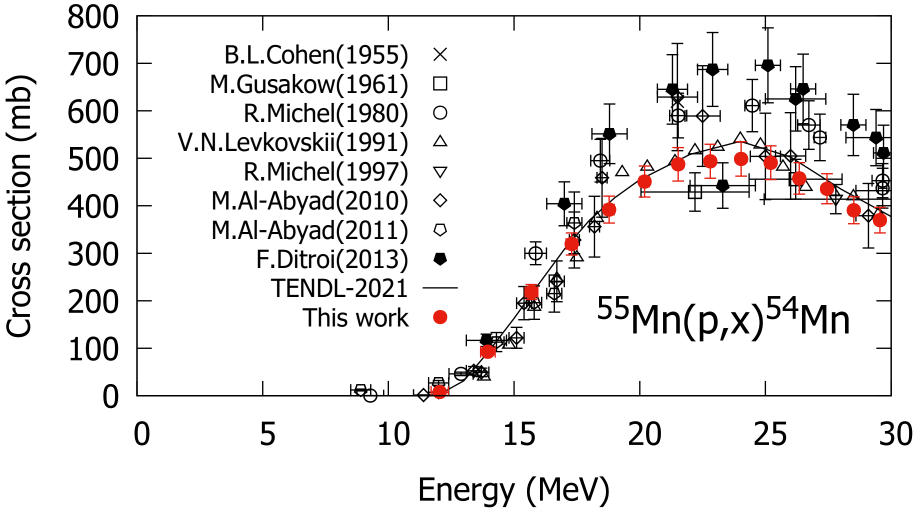

Cross section (mb)
Energy (MeV)
B.L.Cohen(1955)
M.Gusakow(1961)
R.Michel(1980)
V.N.Levkovskii(1991)
R.Michel(1997)
M.Al-Abyad(2010)
M.Al-Abyad(2011)
F.Ditroi(2013)
TENDL-2021
This work
$^{55}Mn(p,x)^{54}Mn$
0
100
200
300
400
500
600
700
800
0
5
10
15
20
25
30

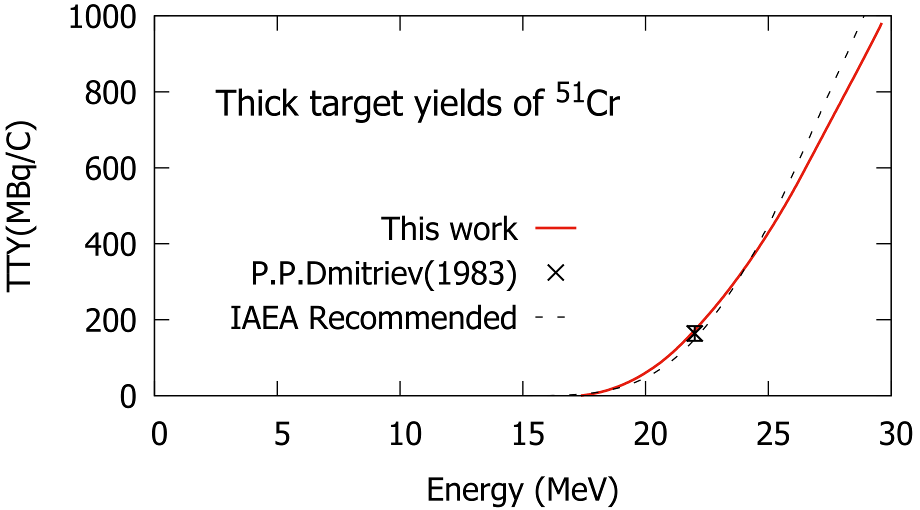

Thick target yields of ^{51}Cr
This work
P.P.Dmitriev(1983)
IAEA Recommended
TTY(MBq/C)
Energy (MeV)
0
200
400
600
800
1000
0
5
10
15
20
25
30

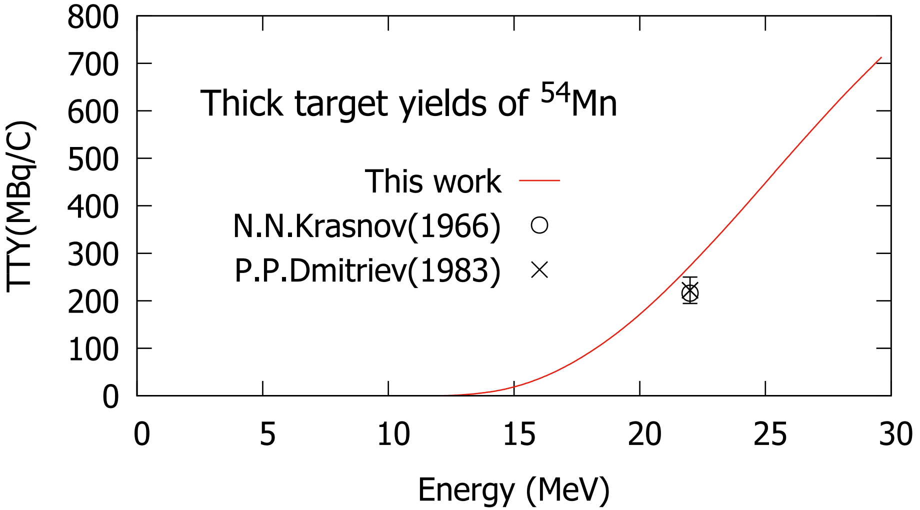

Thick target yields of 54Mn
This work
N.N.Krasnov(1966)
P.P.Dmitriev(1983)
TTY(MBq/C)
Energy (MeV)
0
100
200
300
400
500
600
700
800
0
5
10
15
20
25
30